

Supplementary Information

Stretchable Conductors Based on Three-dimensional Microcoils for Tunable Radio-frequency Antennas

Xinghao Li,^a Jun Cai,^{*a} Xiaozhu Lu,^b Yingying Shi,^a De Gong,^a Donglin Su,^b and Deyuan Zhang^a

a. School of Mechanical Engineering and Automation, Beihang University, Beijing, 100191, China. E-mail: jun_cai@buaa.edu.cn

b. School of Electronics and Information Engineering, Beihang University, Beijing, 100191, China.

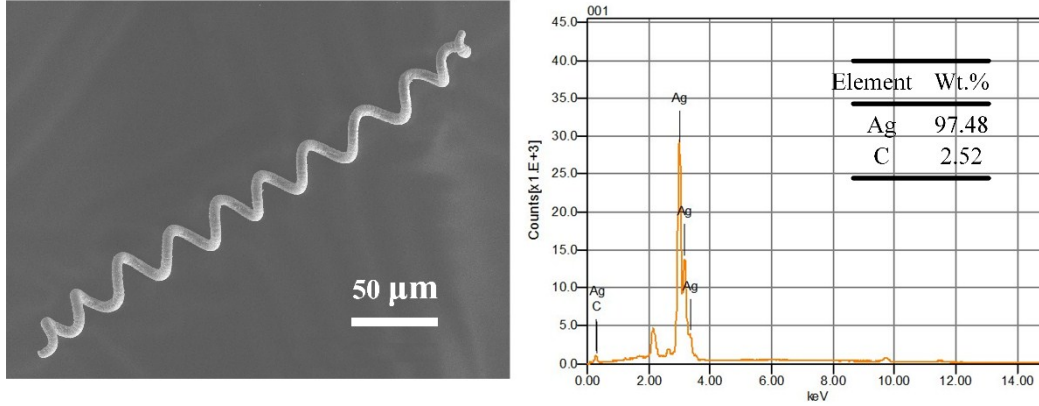


Figure S1 EDS spectra of a silver-coated microcoil. The principal components are silver (up to ~97wt.%) and carbon.

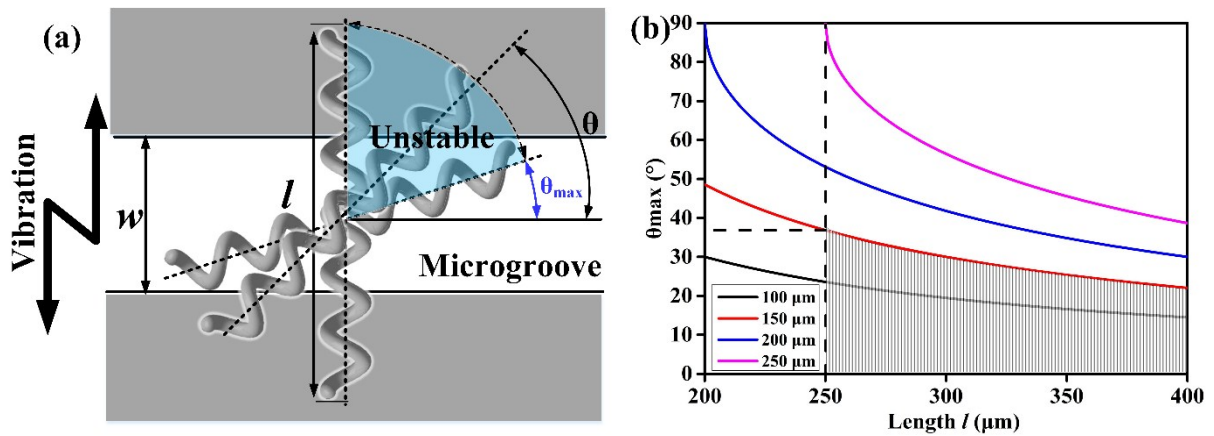


Figure S2 (a) Schematic of microgroove-induced alignment for microcoils. θ is the theoretical deviation angles between the microcoil major axis and the microgrooves. θ_{max} is the maximum theoretical deviation angles. (b) θ_{max} against microcoil length l in different microgrooves. The width w of microgrooves are set as 100 μm , 150 μm , 200 μm and 250 μm , respectively.

Figure S2 demonstrated the mechanism of microgroove-induced alignment. The blue region (Figure S2a) represents the unstable situation of microcoils under a low-frequency vibration (~5Hz). The particles were mixed with ethyl alcohol, and the mixtures were dropped on the masks with parallel microgrooves. The friction force is small on the interface between particles and the

smooth steel plates, so the microcoils were nearly unconstrained on the plates and would be easily driven by the external disturbance. When the low-frequency vibration is applied to the whole devices, the liquid on the plate surface would not simultaneously follow the movement of the plate, due to the fluid inertia effects. The particles would be disturbed by the liquid and adjusted their own attitude. When their major axis is nearly parallel to the grooves, *i.e.* $\theta \leq \theta_{max}$, the microcoils would fall into the microgrooves. Since the groove inwalls could constrain the microcoils to prevent their free rotation, the particles could be in a stable state and directional orientation are achieved. The details of particle alignment and movement are still under investigation. The theoretical maximum deviation angles θ_{max} could be also quantitatively calculated by the equation¹ $\theta = \sin^{-1}(w/l)$. The microcoil length l generally ranges $\sim 200 \mu\text{m}$ to $\sim 400 \mu\text{m}$, so the maximum width of microgroove is chosen as $\sim 200 \mu\text{m}$. Figure S2b demonstrates that the narrower microgrooves and longer microcoils theoretically contribute to smaller θ_{max} or better alignment. In the case of $\sim 150 \mu\text{m}$ grooves, the maximum deviation angle θ_{max} is $\sim 37^\circ$.

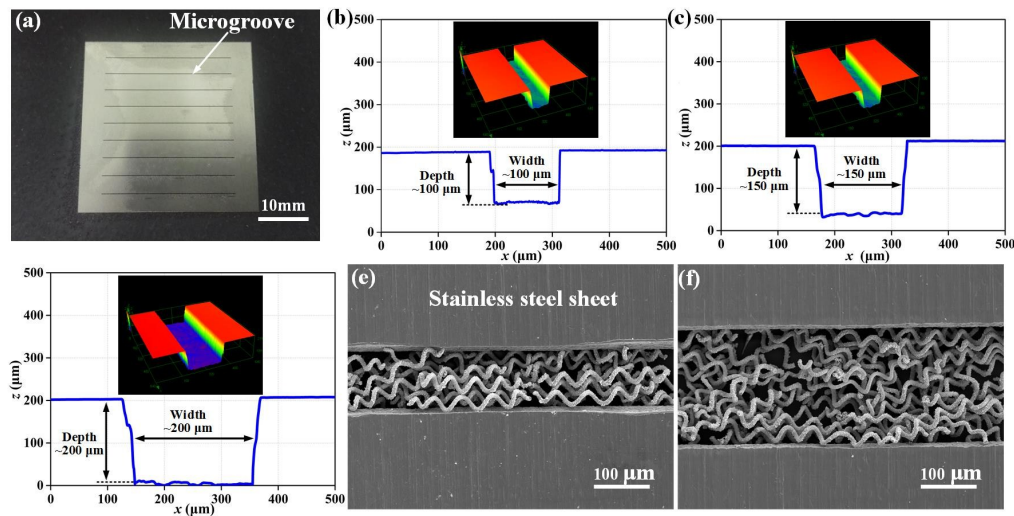


Figure S3 Patterned masks with microgrooves for microcoil alignment. (a) A stainless patterned mask with microgrooves. (b)- (d) The 3D structures of three different microgrooves $\sim 100\ \mu\text{m}$, $\sim 150\ \mu\text{m}$ and $\sim 200\ \mu\text{m}$. The groove width is equal to the depth. (e)- (f) Microcoils in the different grooves with the width of $\sim 100\ \mu\text{m}$ and $\sim 200\ \mu\text{m}$. The directional orientation of microcoils could be achieved via the grooves of $\sim 100\ \mu\text{m}$, while the microcoils seem unordered in the grooves of $\sim 200\ \mu\text{m}$.

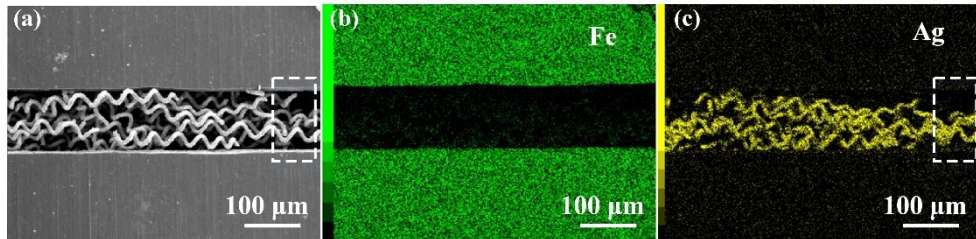


Figure S4 (a) SEM image of aligned microcoils in the microgroove of $\sim 100\ \mu\text{m}$. The inset rectangle area shows that the microcoils insufficiently filled the groove. (b)-(c) Elemental mapping image of aligned microcoils through EDS analysis. The green color represents iron, which is the principal components of the stainless mask. The yellow color represents silver. The whole groove ($\sim 100\ \mu\text{m}$) is so narrow that microcoils could not efficiently fill it up, which leads to discontinuity of long microcoil bars.

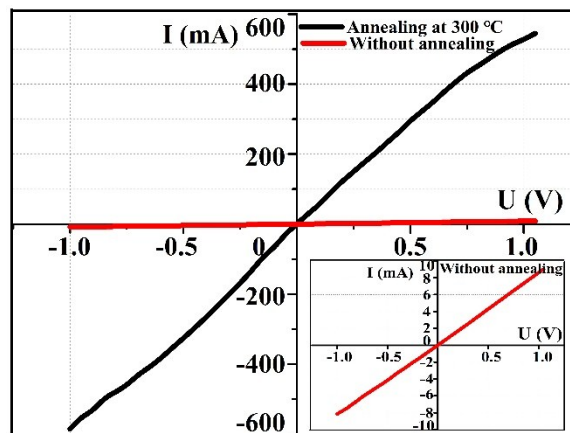


Figure S5 Voltage-current curve of microcoil-based networks annealing at $\sim 300\ \text{°C}$ (black line) and without annealing (red line). The inset shows details of the red line. The conductive networks were $\sim 10\ \text{mm}$ in length with the cross-section of $150\ \mu\text{m} \times 150\ \mu\text{m}$.

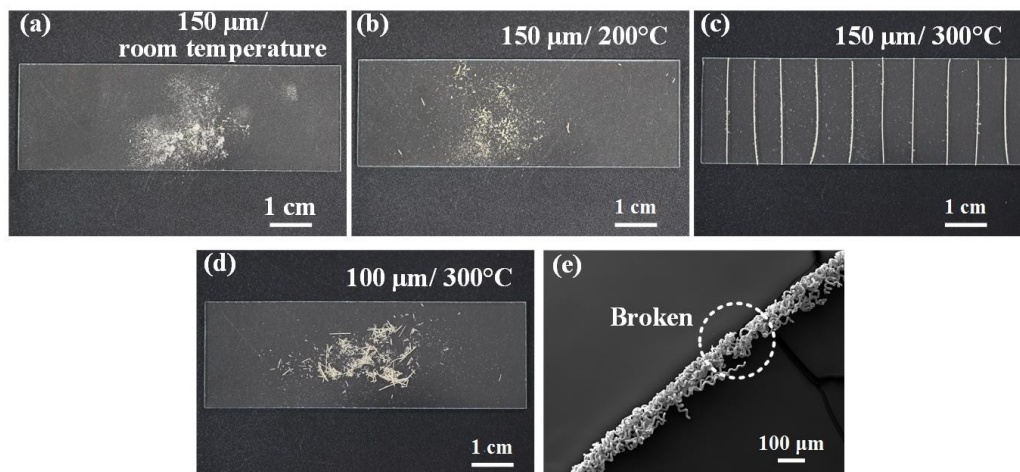


Figure S6 Microcoil-based bars transferred from microgrooves. The microcoils were aligned in different microgrooves and annealed at different temperatures: a) $\sim 150\ \mu\text{m}$, without heat treatment; b) $\sim 150\ \mu\text{m}$, $\sim 200\ ^\circ\text{C}$; (c) $\sim 150\ \mu\text{m}$, $\sim 300\ ^\circ\text{C}$; (d) $\sim 100\ \mu\text{m}$, $\sim 300\ ^\circ\text{C}$. The microcoils were still in powder form when annealed at $\sim 200\ ^\circ\text{C}$ or lower. Yet, when annealed at $\sim 300\ ^\circ\text{C}$, the separated microcoils could be nanowelded together. Furthermore, the microcoil-based bars could be transferred only from the microgrooves of $\sim 150\ \mu\text{m}$. (e) SEM image of a broken bar transferred from microgrooves of $\sim 100\ \mu\text{m}$. The microcoils were annealed at $\sim 300\ ^\circ\text{C}$, yet there was still some discontinuity due to the insufficient filling content.

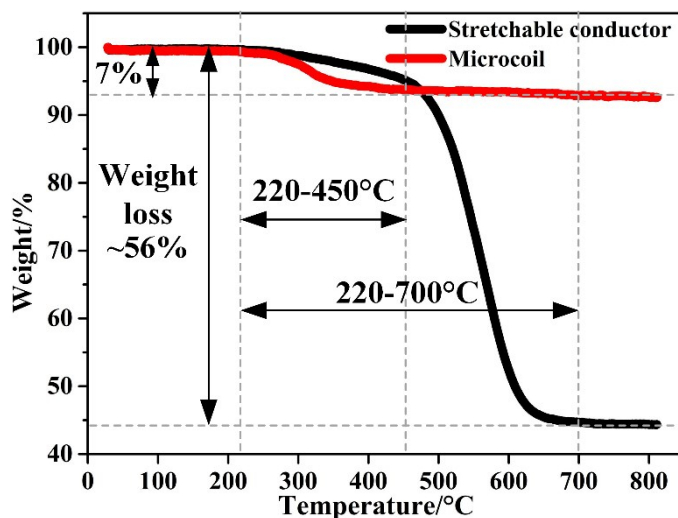


Figure S7 Thermogravimetric analysis (TGA) of conductive microcoils and microcoil-based stretchable conductors.

Pyrolysis tests were carried out in a Simultaneous Thermogravimetric Analyzer (NETZSCH, STA-449F3, Germany). Sample weight loss as functions of time and temperature were recorded continuously. Temperature was ramped from 25 to 810 °C and the heating rates were controlled at 10.0 K/min. The tests were conducted under an argon atmosphere with a flow rate of 80 mL/min. For the thermal behavior of silver-coated microcoil, the weight loss was ~7% within the temperature range of 220-450°C, due to the decomposition of the inner bio-templates: carbohydrates(225-300 °C) and protein(300-400 °C).²⁻³ In the case of microcoil-based composites, the weight fraction of microcoils is ~44% (the biotemplate weight could be neglected compared with the silver coating) and the weight loss mainly results from break down of PDMS within the temperature range of 220-700°C.

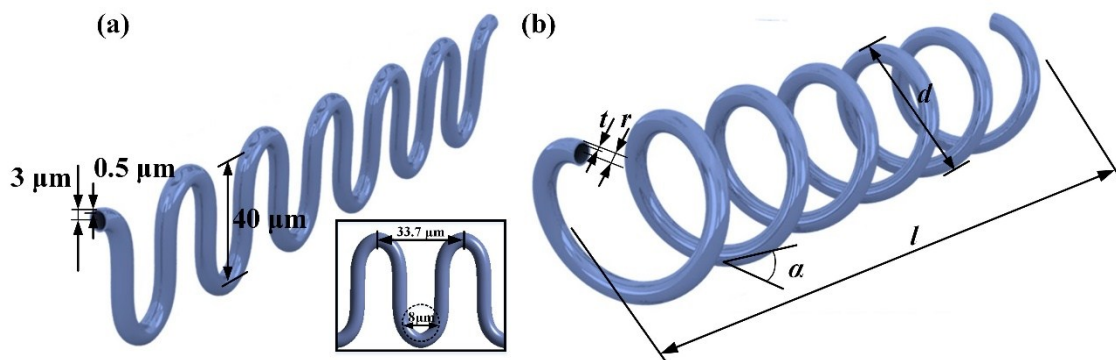


Figure S8 Structural parameters of the 2D wavy layout (a) and 3D microcoil (b).

Corresponding to the feature size of silver-coated *Spirulina*, the 3D microcoil FE model was set as 40 μm in coil diameter (d), 15° in pitch angle (α), 3 μm in wire radius (r), 6 in turn number (N) and 0.5 μm in coating thickness (t).

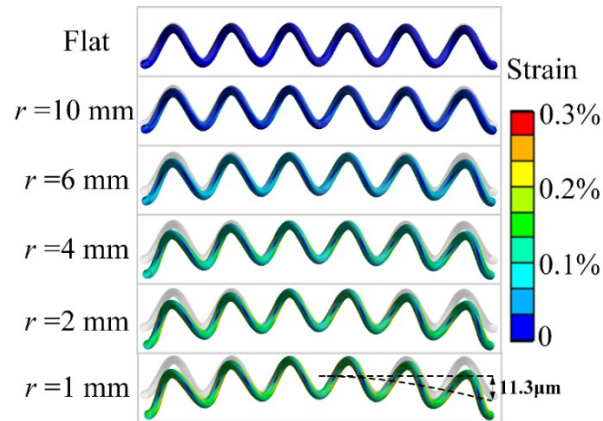


Figure S9 FEA simulation of total equivalent strain for a microcoil during bending deformation.

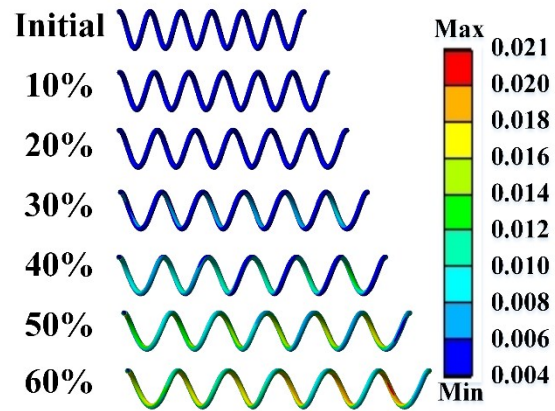


Figure S10 FEA simulation of total strain distribution for a microcoil during the stretch from 0 to 60%.

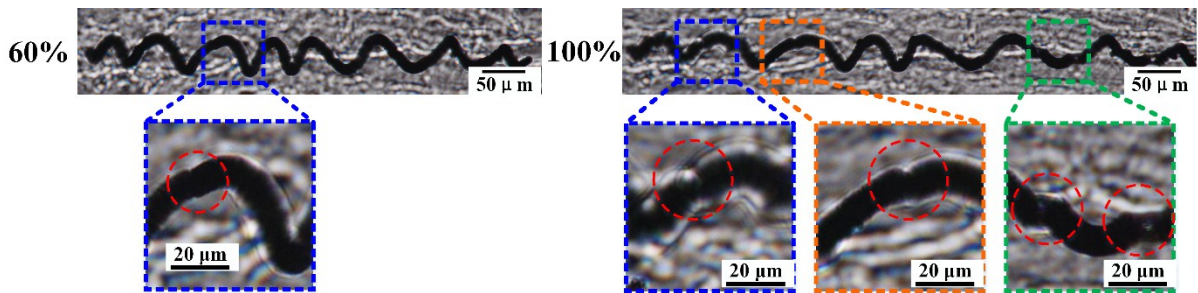


Figure S11 Optical images of a metallic microcoil at the stretch of ~60% and ~100%. Large external tensile stretch leads to the microcoil breakage.

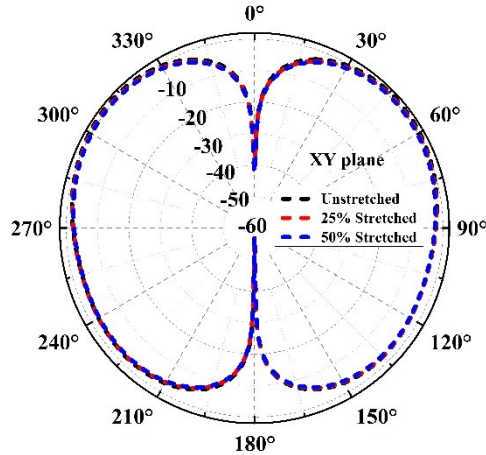


Figure S12 FEA simulation of 2D radiation patterns for the monopole antenna at the stretch of 0, 25% and 50%.

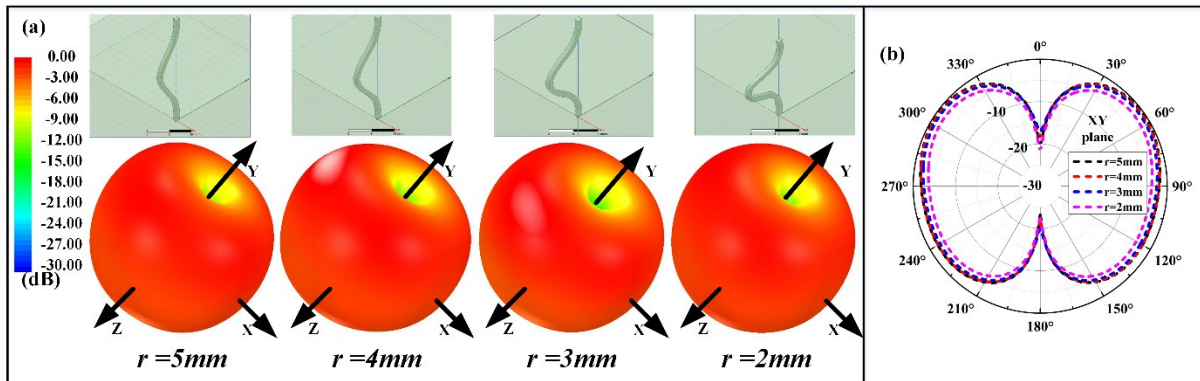


Figure S13 FEA simulation of 3D (a) and 2D (b) radiation patterns for the antenna under bending deformation at the radius of 5 mm, 4 mm, 3 mm and 2 mm.

Reference

- (1) Yang, B.-R.; Cao, W.; Liu, G.-S.; Chen, H.-J.; Noh, Y.-Y.; Minari, T.; Hsiao, H.-C.; Lee,

C.-Y.; Shieh, H.-P. D.; Liu, C. Microchannel Wetting for Controllable Patterning and Alignment of Silver Nanowire with High Resolution. *ACS Appl. Mater. Interfaces* **2015**, *7*, 21433-21441.

(2) Gai, C.; Liu, Z.; Han, G.; Peng, N.; Fan, A. Combustion Behavior and Kinetics of Low-Lipid Microalgae Via Thermogravimetric Analysis. *Bioresour Technol* **2015**, *181*, 148-154.

(3) Ceylan, S.; Topcu, Y.; Ceylan, Z. Thermal Behaviour and Kinetics of Alga *Polysiphonia Elongata* Biomass During Pyrolysis. *Bioresource Technol.* **2014**, *171*, 193-198.